ACES Asian Chemical Editorial Society

doi.org/10.1002/asia.202200325

CHEMISTRY AN ASIAN JOURNAL Research Article

www.chemasianj.org

Special Collection

Modulation of Slow Magnetic Relaxation in Gd(III)-Tetrahalosemiquinonate Complexes

Maja A. Dunstan,[a] Dominic S. Brown,[a] Lorenzo Sorace,[b] Richard A. Mole,[c] and Colette Boskovic*[a]

Abstract: Incorporating lanthanoid(III)-radical magnetic exchange coupling is a possible route to improving the performance of lanthanoid (Ln) single-molecule magnets (SMMs), molecular materials that exhibit slow relaxation and low temperature quantum tunnelling of the magnetization. Complexes of Gd(III) can conveniently be used as model systems to study the Ln-radical exchange coupling, thanks to the absence of the orbital angular momentum that is present for many Ln(III) ions. Two new Gd(III)-radical compounds of formula $[Gd(18\text{-c-}6)X_4SQ(NO_3)].I_3$ (18-c-6 = 18-crown-6, $X_4SQ^{\cdot -}$ = tetrahalo-1,2-semiquinonate, **1**: X = Cl, **2**: X = Br) have been synthesized, and the presence of the dioxolene ligand in its semiquinonate form confirmed by X-ray crystallography, UV-Visible-NIR spectroscopy and voltammetry. Static magnetometry and EPR spectroscopy indicate differences in the low temperature magnetic properties of the two compounds, with antiferromagnetic exchange coupling of $J_{Gd\text{-}SQ} \sim -2.0\ cm^{-1}$ ($\boldsymbol{H}_{ex} = -2J_{Gd\text{-}SQ}(\boldsymbol{S}_{Gd}\boldsymbol{S}_{SQ})$) determined by data fitting. Interestingly, compound **1** exhibits slow magnetic relaxation in applied magnetic fields while **2** relaxes much faster, pointing to the major role of packing effects in modulating slow relaxation of the magnetization.

Introduction

Coordination compounds of the trivalent lanthanoid (Ln) ions have diverse applications, including in areas such as molecular magnetism, magnetocalorics,[1] and magnetic resonance imaging contrast agents,[2,3] which take advantage of the large number of unpaired electrons and large magnetic moments of many Ln(III) ions. In molecular magnetism, lanthanoids with a large magnetic anisotropy and magnetic moment, paired with a doubly degenerate magnetic ground state, allow for slow magnetic relaxation at low temperatures, characteristic of single-molecule magnets (SMMs).[4,5] Typically, the late lanthanoid ions of Tb(III), Dy(III), Ho(III), and Er(III), are the magnetic ions of choice for Ln-SMMs, as their large orbital angular momentum contribution to the magnetic moment can engender a highly anisotropic ground magnetic state.[6] Recently, several notable examples of Ln-SMMs have exhibited slow magnetic relaxation and open magnetic hysteresis loops above liquid nitrogen temperature.[7,8] This opens up applications in data storage and computing, taking advantage of their magnetic bistability, and in quantum computing, due to low temperature quantum tunnelling of the magnetization (QTM).

Efforts to improve the SMM behavior of Ln-SMMs include incorporating magnetic exchange coupling with another spin carrier, such as a radical ligand.[9,10] Radical ligands can be used to magnetically couple multiple Ln(III) ions together, increasing the overall magnetic moment of the resultant complex. Examples include the compounds of formula $[Cp^{Me4H}{}_2Ln_2(\mu\text{-}N_2)]$ which for the Tb(III)-N_2^{3-}-Tb(III) analogue exhibits a magnetic blocking temperature of 20 K, with a large $J_{ex} = -23.1\ cm^{-1}$ ($\boldsymbol{H}_{ex} = -2J_{ex}(\boldsymbol{S}_1\boldsymbol{S}_2)$).[11] Additionally, a small exchange bias can be used to quench zero field QTM in Ln-SMMs, allowing thermal relaxation pathways to dominate.[12,13]

It is, however, generally impossible to determine the magnitude and sign of the Ln-radical magnetic exchange interaction involving Ln(III) ions with large orbital angular momentum by fitting powder magnetic data. Doing so would involve simultaneous determination of the crystal field parameters for the single ion contribution and the exchange parameters, which will in general be anisotropic. For this reason, the magnetic exchange coupling can only be readily determined for Gd(III) analogues, which have an orbitally non-degenerate ground state. Gd(III)-radical compounds have been found to exhibit both ferromagnetic[14–17] and antiferromagnetic[18–22] magnetic exchange interactions between the Gd(III) ion and ligand, with the magnitude of exchange typically on the order of a few wavenumbers. This exchange interaction is typically much smaller than that observed for radical complexes of d-block metals, due to the relative shielded nature of the 4f

[a] M. A. Dunstan, D. S. Brown, Prof. C. Boskovic
School of Chemistry
The University of Melbourne
Parkville VIC 3010 (Australia)
E-mail: c.boskovic@unimelb.edu.au

[b] Prof. L. Sorace
Department of Chemistry, "Ugo Schiff"
Universita Degli Studi Firenze
Via della Lastruccia, 13 - 50019 Sesto Fiorentino (Italy)

[c] Dr. R. A. Mole
Australian Centre for Neutron Scattering
Australian Nuclear Science and Technology Organisation
Locked Bag 2001, Kirrawee DC 2232 (Australia)

Supporting information for this article is available on the WWW under https://doi.org/10.1002/asia.202200325

This manuscript is part of a special collection highlighting Women in Chemistry.

valence orbitals of Ln(III) ions.[10] The current record for Gd(III)-radical exchange is $J_{ex} = -43\ cm^{-1}$ in a Gd-benzene dianion radical complex [Gd_2(μ-BzN_6-Mes)] (BzN_6-Mes = 1,3,5-tris[2′,6′-(N-mesityl)dimethanamino-4′-tert-butylphenyl]benzene).[23]

Of the readily available ligands that can be present as a stable radical, dioxolene and tetraoxolene ligands have found widespread use in transition metal molecular magnetism.[24,25] In Ln(III) molecular chemistry, tetraoxolene ligands have been used to bridge Ln(III) ions in dinuclear species, with the tetraoxolene in both the diamagnetic and radical forms,[26–28] while diamagnetic catecholate ligands have been utilized in both Ln(III) SMM[29–31] and other Ln compounds.[32–35] One group of compounds for which the Ln(III)-dioxolenes are isolable in their semiquinonate redox form are the family of compounds [Ln(Tp)$_2$(DBSQ)] (Tp^- = hydro-tris(1-pyrazolyl)borate, $DBSQ^{\cdot-}$ = 3,5-di-tertbutyl-1,2-semiquinonate).[36,37] Notably, the Gd(III) analogue has a relatively large antiferromagnetic magnetic exchange coupling of $J_{ex} = -5.7\ cm^{-1}$ between the Gd(III) and the $DBSQ^{\cdot-}$ ligand.[36]

Herein we present two coordination compounds [Gd(18-c-6)X_4SQ(NO_3)].I_3 (18-c-6 = 18-crown-6, $X_4SQ^{\cdot-}$ = tetrahalo-1,2-semiquinonate, **1**: X = Cl, **2**: X = Br) synthesized by one-electron oxidation of the parent catecholate analogues with iodine. At the outset of this work, we wished to study the Ln-radical magnetic exchange coupling between Gd(III) and tetrahalo-1,2-semiquinonate radical ligands, to provide insights into the possibility of incorporating tetrahalo-1,2-semiquinonate ligands into Ln(III) SMMs.

Results and Discussion

Synthesis

Precursor catecholate compounds of formula [Gd(18-c-6)X_4Cat(NO_3)].MeCN (X = Cl: **1-Cat**; X = Br: **2-Cat**) were synthesized according to the literature procedure.[30] As these compounds are insoluble in all solvents, conventional methods of chemical oxidation to the semiquinonate analogues were not available. In order to oxidize the catecholate compounds, solid microcrystalline **1-Cat** and **2-Cat** were suspended in a 0.01 M solution of I_2 in chlorobenzene for 4 hours with occasional agitation, yielding compounds **1** and **2**. Iodine was chosen as an oxidizing agent as its oxidizing potential is between the catecholate to semiquinonate and semiquinonate to quinonate oxidation processes measured for **1-Cat** and **2-Cat** from solid state cyclic voltammetry, allowing access to one-electron oxidation. The oxidation reaction also proceeds in toluene or dichloromethane solvent; however, chlorobenzene gave the most consistent products.

The oxidation reaction is accompanied by a gradual change in color of the solid compounds from white to dark brown for **1**, and from yellow to a lustrous black for **2**. The resultant solid compounds are at times contaminated with unoxidized or partially oxidized crystallites, so the compounds were purified by recrystallization. Crude **1** gradually decomposes in the reaction mixture, as well as during recrystallization, perhaps due to overoxidation from residual iodine, and as such **1** was collected by filtration from the reaction mixtures after no more than 4 hours, and recrystallized from dry, degassed solvent. Compound **2** is air and moisture stable and can be recrystallized in air.

Compound **2** is obtainable as several solvatomorphs, as well as a solvent-free polymorph, depending on the solvents and reaction/recrystallization conditions used. However, **1** was only obtained as a solvent-free polymorph. Efforts to generate the same polymorph for both compounds were unsuccessful, and we elected to characterize the solvent-free polymorph of both compounds.

Crystallography and structure description

Both **1** and **2** crystallize in the monoclinic space group $P2_1/n$, however, the unit cell differs between the two (Table 1). Both compounds crystallize with one cationic coordination complex and one triiodide anion per asymmetric unit. Both compounds have strong X-ray absorption due to the Gd and I atoms, and as such, the structures have high minimum and maximum electron density in the structures. Compound **2** has additionally high X-ray absorption from the Br atoms. Powder X-ray diffraction data were obtained for bulk samples of both **1** and **2** and compared

Table 1. Crystal data for **1** and **2**.

	1	**2**
Empirical formula	$C_{18}H_{24}NO_{11}Cl_4I_3Gd$	$C_{18}H_{24}NO_{11}Br_4I_3Gd$
Formula weight	1110.13	1287.97
Temperature/K	100.00(10)	99.99(10)
Crystal system	monoclinic	monoclinic
Space group	$P2_1/n$	$P2_1/n$
a/Å	11.5435(5)	8.0719(2)
b/Å	16.5725(5)	17.4652(4)
c/Å	16.5351(5)	22.1846(5)
β/°	102.244(4)	97.767(2)
Volume/Å^3	3091.29(19)	3098.83(13)
Z	4	4
ρ_{calc}/g cm^{-3}	2.386	2.761
μ/mm^{-1}	41.057	10.338
F(000)	2072.0	2360.0
Crystal size/mm^3	0.117×0.089×0.046	0.163×0.078×0.068
Radiation	CuK_α (λ = 1.54184)	MoK_α (λ = 0.71073)
2Θ range/°	7.642 to 153.828	4.378 to 61.764
Index ranges	$-14 \le h \le 14$, $-18 \le k \le 20$, $-20 \le l \le 12$	$-11 \le h \le 9$, $-19 \le k \le 25$, $-28 \le l \le 27$
Reflections collected	26112	30204
Independent reflections	6278 [R_{int} = 0.1188, R_{sigma} = 0.0730]	7925 [R_{int} = 0.0376, R_{sigma} = 0.0388]
Data/restraints/parameters	6278/0/343	7925/0/343
Goodness-of-fit on F^2	1.000	1.041
Final R indexes [$I \ge 2\sigma(I)$]	R_1 = 0.0785, wR_2 = 0.2039	R_1 = 0.0411, wR_2 = 0.1120
Final R indexes [all data]	R_1 = 0.0928, wR_2 = 0.2195	R_1 = 0.0533, wR_2 = 0.1169
Largest diff. peak/hole/e Å^{-3}	2.42/−2.28	3.81/−4.11

to data simulated from single crystal X-ray diffraction, confirming phase purity (Figures S1–2).

The Gd(III) center in both compounds has an $\{O_{10}\}$ coordination sphere, made up of a bidentate nitrate ligand, an equatorial 18-crown-6 ligand, and a X_4-semiquinonate ligand (Figure 1). The coordination geometry at the Gd(III) center in **1** has a SHAPE[38] distortion parameter closest to a distorted sphenocorona, although the distortion parameters are close to that for a bicapped square antiprism. For **2**, the coordination geometry at the Gd(III) center is instead closest to a distorted bicapped square antiprism (see Table 2).

Bond length analysis can be used to determine the oxidation state of redox-active ligands.[39] Comparison of the dioxolene C–C and C–O bond lengths of **1** and **2** with the Gd(III)-catecholate compound **1-Cat** and with literature $Cl_4SQ^{\cdot-}$ compounds[40,41] allows assignment of the oxidation state. The bond lengths for the X_4-dioxolene ligands (Table 2) are consistent with a semiquinonate oxidation state, with shorter C–O bond lengths and C–C bond lengths deviating from the ~1.4 Å C–C bond length in the catecholate oxidation state, consistent with loss of aromaticity of the ring and an increase in double bond character in the C–O bonds. In addition, the semiquinonate ligands are slightly buckled in both structures. For **1**, there are no apparent directional packing interactions between the Gd complex and the triiodide counterion and neighboring complexes (Figure S3). For **2**, there is a stacking motif, where Br_4-semiquinonate radical ligand and I_3^- counterion alternate (Figures S4–5), with the closest Br, I, and C atoms separated by the sum of the van der Waals radii +0.3 Å. The shortest intermolecular Gd…Gd distance in **2** is also slightly shorter than that in compound **1** with distances of 7.7395 Å and 8.0757 Å, respectively.

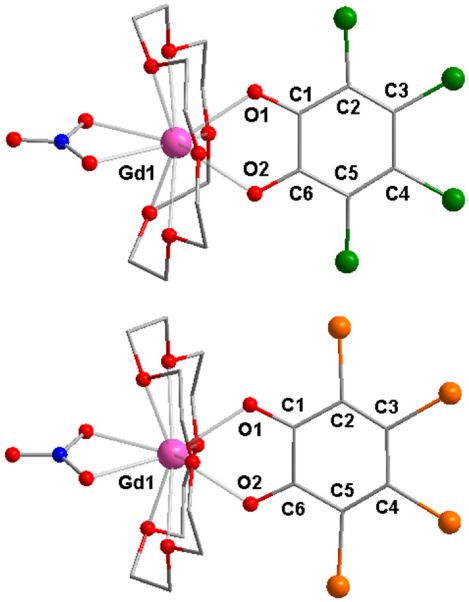

Figure 1. Crystallographic representation of **1** (top) and **2** (bottom). Color code: Gd (pink), C (grey), N (blue), O (red), Cl (green), Br (orange). Hydrogen atoms have been omitted for clarity.

Table 2. Selected intra-atomic bond lengths, intermolecular distances and SHAPE[38] parameters for **1**, **2**, and **1-Cat**.

	1	2	1-Cat[a]
Distance/Å			
Ave. Gd–O(diox)	2.387(9)	2.377(7)	2.276(10)
Ave. C–O(diox)	1.272(16)	1.275(12)	1.324(17)
C1–C6	1.446(14)	1.452(10)	1.391(15)
Ave. C1–C2/C5–C6	1.434(14)	1.462(14)	1.405(19)
Ave. C2–C3/C4–C5	1.376(19)	1.376(14)	1.406(21)
Intermolecular Gd···Gd	8.0757(7)	7.7395(5)	–
SHAPE parameters			
bc-SAPR[b]	2.891	2.634	–
SPC[c]	2.457	3.152	–

[a] Equivalent dioxolene bonds. Diox = $X_4cat^{2-}/X_4SQ^{\cdot-}$. [b] Bicapped square antiprism. [c] Sphenocorona.

Spectroscopy

The compounds **1** and **2** are both darkly colored and solvatochromic in solution due to the presence of the I_3^- anion. The solution state electronic absorption spectra of both analogues were measured in acetonitrile (Figure 2), as well as the solution spectrum of Bu_4NI_3 (Figure S8), to identify the bands due to the triiodide anion.

The intense absorption bands at 291 nm and 361 nm observed for both **1** and **2** can be assigned as characteristic I_3^- bands, from comparison with the spectrum of the Bu_4NI_3. The remaining bands for both compounds are assigned as ligand-based transitions, and no characteristic sharp f-f transitions are observed for the Gd(III) ion. Of note in the ligand bands is the structured feature centered at 934 (**1**) and 920 nm (**2**) with a low extinction coefficient of ~200 $L\,mol^{-1}\,cm^{-1}$, which is characteristic of a semiquinonate ligand,[42] and is absent in the spectra of the parent compounds **1-Cat** and **2-Cat**.[30]

Additionally, the FT-IR spectra of both **1** and **2** (Figures S6–7) show a strong similarity with the spectra reported for **1-Cat** and **2-Cat**,[30] suggesting the overall structure remains unchanged upon oxidation. A shift in the C–O vibrations to higher frequency (ν ~1450–1550 cm^{-1}) is consistent with a shortening

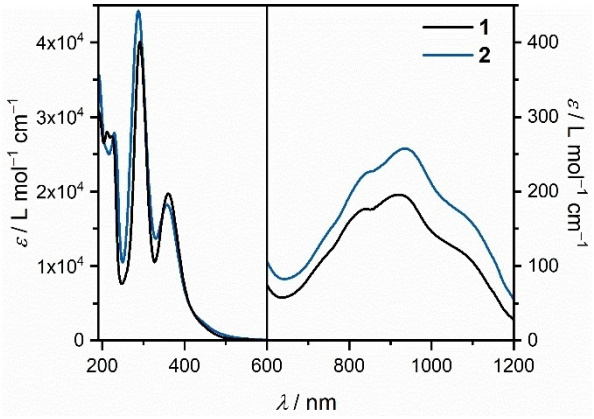

Figure 2. Electronic absorption spectra of **1** (black) and **2** (blue) in acetonitrile.

of the C–O bond upon ligand oxidation from catecholate to semiquinonate.[24]

Electrochemistry

Voltammetric measurements of **1** and **2** were performed in acetonitrile solution with Bu_4NPF_6 supporting electrolyte to further confirm the redox state of the two compounds. Rotating disk electrode voltammetry was used to determine the position of zero current accurately, as there are closely spaced processes in that region (Figures S9–11). The cyclic voltammograms of **1** and **2** are shown in Figure 3. Four identifiable processes can be observed for both analogues, an irreversible reduction **I**, a quasireversible reduction **II**, a quasireversible oxidation **III**, and an irreversible oxidation **IV**. Worth noting is that processes **II** and **III** show signs of reversibility, however, the close spacing of processes **II**, **III** and **IV** doesn't allow for accurate analysis of the peak-to-peak separation, and for all processes observed for **1** and **2**, only the peak anodic or peak cathodic potentials (E_{pa} and E_{pc}) are tabulated (Table 3). From comparison with a cyclic voltammogram of Bu_4NI_3 performed in the same conditions (Figure 2), processes **I** and **III** can be assigned as triiodide based redox processes as shown in Scheme 1. The potentials of **I** and **III** are shifted slightly between analogues, so to confirm the processes in **1** and **2** are the same as those in the Bu_4NI_3, excess Bu_4NI_3 was added to a solution of **2** during measurement (Figure S8). The remaining two processes for **1** and **2** can then be assigned as dioxolene-based from comparison with the redox processes observed in the parent compounds **1-Cat** and **2-Cat**, as a one-electron reduction of the $X_4SQ^{\cdot-}$ ligand to the X_4Cat^{2-} redox state; and a one-electron oxidation of the $X_4SQ^{\cdot-}$ to the X_4Q^0 (X_4Q^0 = tetrahaloquinone) (Scheme 1).

The relative positions of the dioxolene processes and the I_3^-/I_2 couple confirm the choice of I_2 as an ideal oxidizing agent to selectively generate one-electron oxidized compounds **1** and **2**.

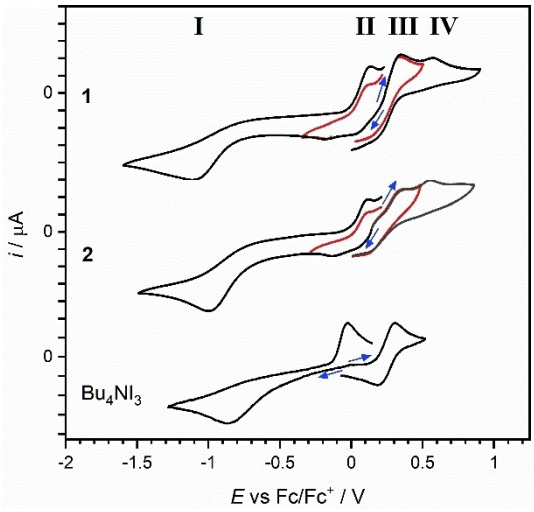

Figure 3. Cyclic voltammetry of **1** (top), **2** (middle), and Bu_4NI_3 (bottom) at 100 mV/s scan rate at 10^{-3} M in 0.1 M Bu_4NPF_6 in CH_3CN.

Table 3. Electrochemical potentials of oxidation and reduction processes for **1**, **2**, and Bu_4NI_3 referenced to the Fc/Fc^+ couple.

Compound	E_{pa} or E_{pc} [V] I	II	III	IV
1	−1.108	−0.188	0.353	0.563
2	−1.003	−0.133	0.371	0.553
Bu_4NI_3	−0.863	–	0.243[a]	–

[a] E_m.

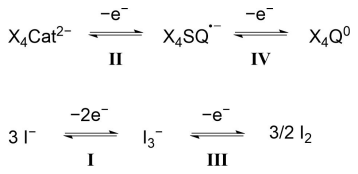

Scheme 1. Redox processes observed in voltammetry measurements of **1**, **2**, and Bu_4NI_3.

Static magnetometry and EPR spectroscopy

Static magnetic data were obtained for both **1** and **2** to investigate the magnetic properties and potential magnetic exchange coupling between the Gd(III) ion and semiquinonate ligand (Figure 4). The room temperature magnetic susceptibility temperature products ($\chi_M T$) for both **1** and **2** have values of 8.25 and 8.33 $cm^3\,K\,mol^{-1}$, respectively, compared to the expected theoretical value of 8.25 $cm^3\,K\,mol^{-1}$ for an uncoupled Gd(III) ($S_{Gd}=7/2$, $g=2.00$) and one radical ($S_{SQ}=1/2$, $g=2.00$). The $\chi_M T$ profile for both is relatively constant until about 75 K, where it slowly starts to decrease with decreasing temperature.

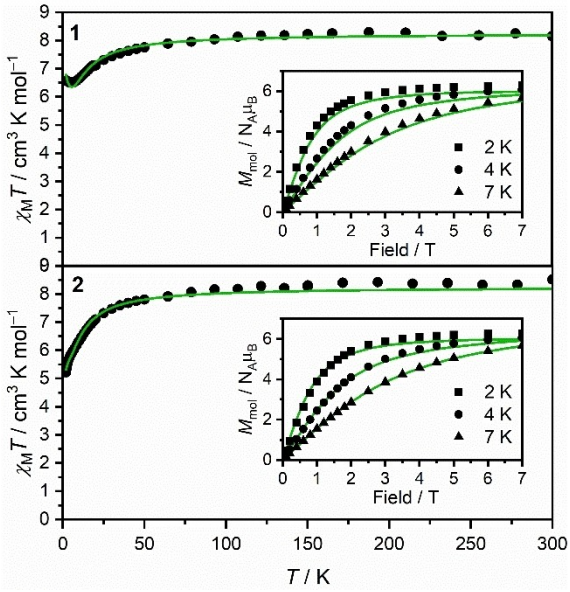

Figure 4. Static (dc) magnetic susceptibility temperature product with temperature in an applied field of $H_{dc}=1{,}000$ Oe for **1** (top) and **2** (bottom). Insets: magnetization with field at specified temperatures. Green lines are simulated profiles from fits as described in the text.

As a Gd(III) ion has a ground ^8S spectroscopic term without orbital angular momentum, the $\chi_M T$ for an isolated Gd(III) ion is expected to remain constant throughout the whole temperature range. The observed deviation at relatively high temperature from this behavior suggests an antiferromagnetic exchange interaction between the Gd(III) and the radical ligand. It is interesting to note that below 20 K, the behavior for the two analogues begins to diverge (Figure S10). The $\chi_M T$ product for **1** decreases slowly until reaching a minimum at 5 K, below which it increases slightly until 2 K, suggesting a weak intermolecular ferromagnetic exchange interaction between neighboring complexes. In contrast, the $\chi_M T$ profile of **2** decreases much more rapidly than that of compound **1** below 20 K, and decreases more rapidly again below 4 K, suggesting a weak intermolecular antiferromagnetic exchange interaction between neighboring molecules. We note that the difference in magnetic behavior cannot be attributed to ferromagnetic impurities in either sample, since measurement of M vs H at 100 K did not show any deviation from purely paramagnetic behavior (Figure S11–12). The field dependent magnetization was also measured for both analogues at low temperature (Figure 4). For both complexes the values saturate at 6.28 μ_B at 2 K. This is lower than that expected for an uncoupled Gd(III) ion (7 μ_B) but in reasonable agreement with expectations for a fully populated $S=3$ state, thus being in agreement with an antiferromagnetic exchange interaction between the Gd(III) and semiquinonate ligand in both compounds. The reduced magnetization for both analogues all overlay well, indicating that the anisotropy of the Gd-semiquinonate systems is still very small, as expected for a Gd(III) system (Figure S12–13).

To further probe the low temperature behavior of the two analogues, X-band EPR spectra were obtained for powder samples at 5 K. For both analogues, the low temperature data are consistent with an $S=3$ with a rhombic zero field splitting, as previously observed for the Gd-semiquinonate system [Gd-(Tp)$_2$(DBSQ)].[43] The spectra of **1** and **2** differ at low temperature, suggesting small differences in the ZFS of the $S=3$ state.

Fits of the static magnetic data and EPR spectra were performed for the two analogues using the software PHI to obtain the magnetic exchange coupling $J_{Gd\text{-}SQ}$ in, as well as an estimate of the zero field splitting of the Gd(III) ion.[44] Initial fits of the magnetization data at the three temperatures and the dc magnetic susceptibility above 10 K with g_{Gd} and g_{SQ} fixed to 2.0 give for **1** a magnetic exchange coupling $J_{Gd\text{-}SQ}$ between the Gd(III) ion and the semiquinonate radical of -1.9 cm^{-1}, using the exchange Hamiltonian:

$$\hat{H}_{ex} = -2J_{Gd-SQ} \cdot \hat{S}_{Gd} \cdot \hat{S}_{SQ} \quad (1)$$

To reproduce the low temperature ($T < 5$ K) dc magnetic susceptibility an additional term that takes into account intermolecular exchange interactions is required, J_{MF}, using the mean-field approximation:

$$\chi_{MF} = \frac{\chi_{calc}}{1 - \left(\frac{J_{MF}}{N_A \mu_B{}^2}\right)\chi_{calc}} \quad (2)$$

which only acts on the dc magnetic susceptibility. Fits of the magnetization data and the full temperature range of the magnetic susceptibility with both J_{MF} and $J_{Gd\text{-}SQ}$ give a $J_{Gd\text{-}SQ} = -2.1$ cm^{-1}. To fully reproduce the EPR spectrum, the following spin Hamiltonian was used:

$$\hat{H}_{EPR} = -2J_{Gd-SQ} \cdot \hat{S}_{Gd} \cdot \hat{S}_{SQ} + \hat{S}_{Gd} \cdot \boldsymbol{D}_{Gd} \cdot \hat{S}_{Gd} + \mu_B \left(g_{Gd}\hat{S}_{Gd} + g_{SQ}\hat{S}_{SQ}\right) \cdot B \quad (3)$$

where we neglected the effect on the spectrum of the dipolar and anisotropic exchange interactions. The $\boldsymbol{D}_{Gd}$ tensor was parametrized in terms of the axial ($D = 3/2D_{zz}$) and rhombic ($E = 1/2(D_{xx}\text{-}D_{yy})$) parameters. A combined fit of the magnetic data and EPR spectrum (green lines, Figures 5 and 6) was performed, giving the best fit parameters in Table 4. We note that the quality of the EPR simulations are insensitive to the sign of D, due to the thermal energy resulting in the sublevels of the ground multiplet being essentially equipopulated at 5 K. The powder EPR data are also insensitive to the sign of E. As the single-ion ZFS parameters obtained are so small, fits of just the magnetic data alone are equally good with D and E included, or neither included, with the values of $J_{Gd\text{-}SQ}$ *and* J_{MF} obtained in each fit essentially the same (Table S1).

The magnetic and EPR data for compound **2** were fit in the same manner, with an antiferromagnetic $J_{Gd\text{-}SQ} = -1.7$ cm^{-1} obtained from fits of the magnetization data as well as from the combined fits of the magnetization, dc magnetic susceptibility, and EPR data, using the various combinations as described for

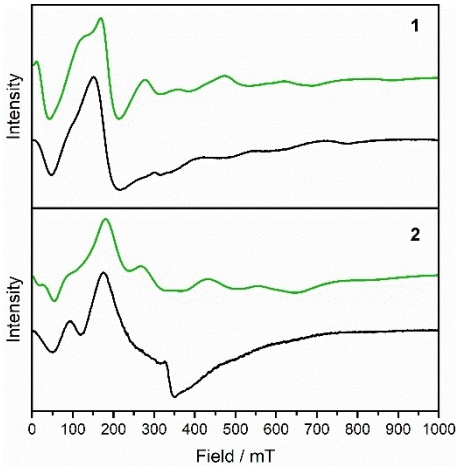

Figure 5. Low temperature (5 K) X-band EPR spectra of **1** (top) and **2** (bottom). Green lines are simulated profiles from data fits as described in the text.

Table 4. Fitting parameters obtained from PHI[44] fitting used to simulate magnetometric & EPR spectroscopic data.

	1	2
D/cm^{-1}	−0.14(1)	−0.11(1)
E/cm^{-1}	−0.014(1)	−0.013(1)
$J_{Gd\text{-}SQ}$/cm^{-1}	−2.1(2)	−1.7(2)
J_{MF}/cm^{-1}	0.011(2)	−0.011(3)

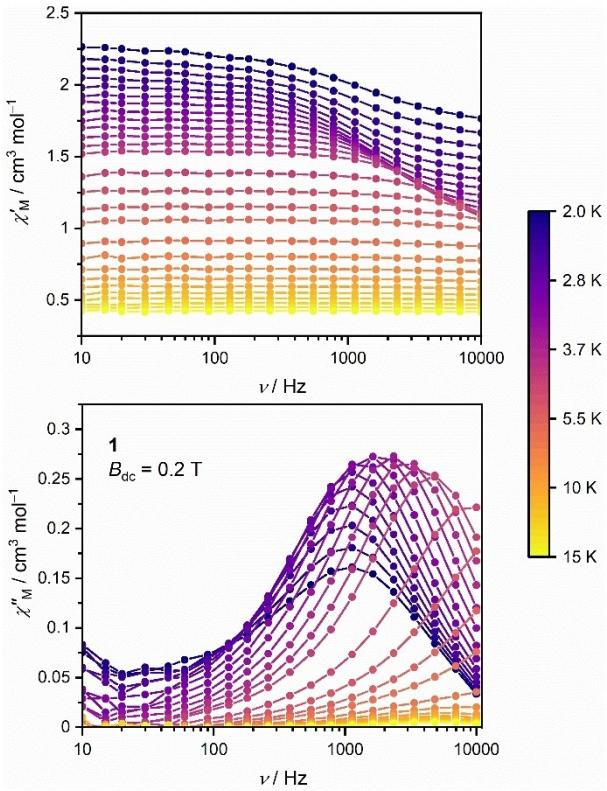

Figure 6. In-phase (top) and out-of-phase (bottom) components of the ac magnetic susceptibility of **1** measured in an applied magnetic field of B_{dc} = 0.2 T.

compound **1** (Table 4, Table S2). The EPR spectrum is reproduced less well for **2**. However, this is mainly due to the feature in the region near ~340 mT, which could not be satisfactorily reproduced by the simulations, and we attribute to a g = 2.00 paramagnetic impurity in the sample. As such, the ZFS parameters obtained for **2** are approximate, but they are consistent with the value of the same parameters obtained for **1**.

For both **1** and **2**, the values of $|D|$ and $|E|$ are similar between the analogues, which is consistent with the similar coordination geometry of the Gd(III) centers in the two analogues. It should be noted that as the values of D and E are small, and the EPR features quite broad, the ZFS parameters cannot be determined with a good degree of accuracy and are an estimate only. However, they are in very good agreement with values reported for the literature Gd(III)-semiquinonate compound [Gd(Tp)$_2$(DBSQ)].[43] Additionally, the magnitude of $J_{Gd\text{-}SQ}$ is similar for the two analogues as expected. The values of $J_{Gd\text{-}SQ}$ of ~ −2 cm^{-1} are about a third of the exchange coupling observed for [Gd(Tp)$_2$(DBSQ)].[36] We tentatively attribute this difference to the electron-withdrawing character of the halo-substituent reducing the electron density on the coordinated O atoms compared to the *tert*-butyl groups on DBSQ·$^-$. This affords poorer spatial overlap between magnetic orbitals responsible for the direct exchange interaction, as observed for transition-metal semiquinonate compounds.[45,46]

Dynamic magnetometry

The fits of the static magnetic data and EPR spectra suggest a $|D|$ in the range 0.10–0.14 cm^{-1} for **1** and **2**. In literature, Gd(III) compounds with $|D|$ values of a similar magnitude have been observed to exhibit slow magnetic relaxation in applied magnetic fields.[47–49] We therefore measured the ac magnetic susceptibility of **1** and **2** to check for slow magnetic relaxation. Scans of the out-of-phase magnetic susceptibility at 2.0 K with varying magnetic field revealed an optimal applied magnetic field of B_{dc} = 0.2 T for compound **1** (Figure S14), while compound **2** exhibits no peaks in the out-of-phase magnetic susceptibility in fields up to 0.3 T and was not measured further (Figure S15). The ac magnetic susceptibility for compound **1** was measured in the range 2–15 K, with temperature dependent peaks in the out-of-phase component observed up to 6 K, indicative of slow magnetic relaxation (Figure 6).

The out-of-phase component of the magnetic susceptibility for **1** was fit with the Debye equation to give the relaxation rate with temperature (Figure 7). A fit of the magnetic relaxation rate (τ^{-1}) should in principle be performed using Equation 4:

$$\tau^{-1} = AT + \tau_{QTM}^{-1} + \tau_0^{-1}\frac{U_{eff}}{kT} + CT^n \quad (4)$$

Where A represents direct relaxation coefficient, τ_{QTM}^{-1} is the rate of QTM, τ_0^{-1} is the Orbach coefficient, U_{eff} the effective energy barrier to Orbach relaxation, C the Raman coefficient and n the Raman exponent. It should be noted that the relaxation behavior of Gd-SMMs previously reported has been fit using both Raman and Orbach relaxation processes.[50–57] The EPR measurements for **1** clearly indicate that $|D_{Gd}| \approx 0.10$ cm^{-1}, implying an extension of the ground S = 3 multiplet of ca. 1.5 cm^{-1}. Fits of the relaxation rate incorporating an Orbach relaxation term gives U_{eff} values > 8 cm^{-1}, which are unreasonably large and can safely be discarded on the basis of the EPR results. As the ac magnetic susceptibility data were measured in an external applied field, we may consider the QTM to be quenched, and as such a fit was performed with a combination of direct relaxation and Raman relaxation processes (fit 1,

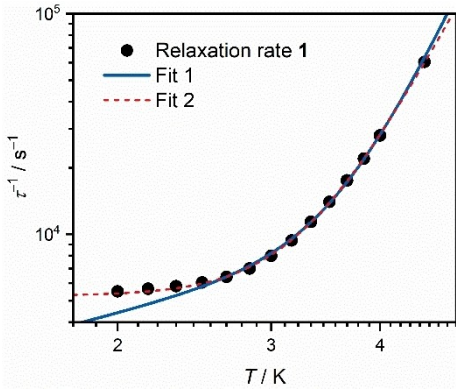

Figure 7. Relaxation rates with temperature for **1** in as determined by ac magnetic susceptibility measurements (data points), fit 1 (blue line) and fit 2 (dashed red line) as described in the text.

Figure 7, Table 5). This fit gives $A = 2181(67)\ K^{-1}$, $C = 0.135(6)\ s^{-1}K^{-n}$, and $n = 8.57(32)$. However, the lowest temperature data are not well fit. Alternatively, the relaxation rates can be slightly better fit using a Raman relaxation term and a QTM relaxation term (fit 2, Figure 7, Table 5), with a $C = 0.882(89)\ s^{-1}K^{-n}$, $n = 7.34(7)$, and $\tau_{QTM}^{-1} = 5.25(6) \times 10^3\ s^{-1}$. The applied field used for the measurement of the magnetic susceptibility may not have been large enough to remove QTM completely. For the second fit, the Raman relaxation with a $T^{\sim 7}$ dependence is consistent with a system with integer spin, which the Gd- semiquinonate system is, if treated as the $S = 7/2$ of the Gd(III) antiferromagnetically coupled with the $S = 1/2$ of the semiquinonate.[58]

The analysis of the dynamic magnetic properties indicates a stark difference in the behavior of the two analogues. *A priori*, this might be attributed to the difference in the magnitude of the Gd-semiquinonate exchange coupling in the compound, as the halogenation on the semiquinonate ligand varies between the two. However, the $Cl_4SQ^{\cdot -}$ and $Br_4SQ^{\cdot -}$ ligands are not expected to behave significantly differently, with both Cl and Br having similar electronic properties, as observed in the related catecholate compounds [Ln(18-c-6)X_4Cat(NO_3)].MeCN.[30] Indeed, the fits of the $J_{Gd\text{-}SQ}$ for both **1** and **2** give values of near $-2\ cm^{-1}$. A second reason for the observed difference might be a different ZFS of the Gd(III) center, due to differences in the Gd(III) coordination geometry and ligand field strength of the two semiquinonates. Indeed, it has been observed for Ln-SMMs incorporating the later Ln(III) ions such as Tb(III), Dy(III), and Er(III), that slight changes in the coordination sphere due to crystal packing or ligand modification can result in large changes in the crystal field splitting and slow magnetic relaxation.[59–62] However, the coordination geometry of the Gd(III) center in **1** and **2** is very similar, and the EPR determined values of $|D|$ and $|E|$ are small and very close to each other, allowing us to discard also this possibility. In contrast, the major difference between the two compounds lies in the crystal packing. This could lead to changes in the slow magnetic relaxation due to the spectrum of phonon modes that allow slow magnetic relaxation. This mechanism should affect only the dynamic magnetic properties, and not the static properties, as observed recently for solvatomorphs of the parent **2-Cat** analogues.[29] However, the difference in the crystal packing also leads to different intermolecular interactions in the two compounds. This is observed as the difference in the low temperature magnetic susceptibility data, which was modelled with a mean-field interaction parameter J_{MF} that is of the same magnitude, but notably of different signs in compounds **1** and **2**. One may then speculate that the intermolecular antiferromagnetic exchange coupling in compound **2** quenches the slow magnetic relaxation completely in the measured field range, while for compound **1**, the longer Gd···Gd distance and lack of a semiquinonate ···I_3^-··· semiquinonate interaction leads to a different intermolecular exchange interaction, with less effect on the slow magnetic relaxation. To explore the role of intermolecular interactions, ac magnetic susceptibility measurements were performed on both compounds as frozen solutions (Figures S17–18). The field dependence of the ac magnetic susceptibility in the region between 10 and 1,000 Hz for both compounds exhibits the onset of a peak in the out-of-phase response at $\nu > 1{,}000$ Hz with increasing fields, consistent with the presence of the field-dependent peaks in **1** in the solid state. Notably, the ac susceptibility profiles of **1** and **2** are very similar when measured as a frozen solution, suggesting both compounds exhibit slow magnetic relaxation in applied magnetic fields. This solution behavior confirms that solid state effects, related to intermolecular interactions or a different phonon spectrum, are the major factor in the difference in dynamic magnetic properties in the crystalline state.

Table 5. Relaxation parameters obtained from fitting the ac susceptibility data for **1**.

	Fit 1	Fit 2
$C/s^{-1}\ K^{-n}$	0.135(6)	0.882(89)
n	8.57(32)	7.34(7)
A/K^{-1}	2181(67)	–
τ_{QTM}^{-1}/s^{-1}	–	$5.25(6) \times 10^3$

Conclusion

Two new mononuclear Gd(III)-semiquinonate compounds **1** and **2** have been synthesized from the insoluble Gd(III)-catecholate analogues by a one-electron oxidation of the dioxolene ligand using iodine. The presence of the radical semiquinonate ligand was confirmed through bond length analysis using single-crystal X-ray diffraction data. Additional evidence for the semiquinonate oxidation state was found from a characteristic absorption band in the UV-Visible-NIR spectra, and from observation of $Cat^{2-}/SQ^{\cdot -}$ and $SQ^{\cdot -}/Q^0$ redox processes in the electrochemical measurements. Analysis of the crystallographic data show that **1** and **2** have different crystal packing and therefore different intermolecular interactions, leading to observed differences in the magnetic properties at low temperature. Both compound **1** and **2** display an intramolecular antiferromagnetic magnetic exchange interaction between the Gd(III) and seminquinonate ligand, fit to $J_{Gd\text{-}SQ} = -2.1\ cm^{-1}$ and $-1.8\ cm^{-1}$, respectively. This is consistent with the observation of antiferromagnetic exchange in other reported Ln-semiquinonate and Ln-tetraoxolene radical compounds.[27,28,36,37,64] The determination of Ln(III)-radical exchange coupling is important for the design of Ln(III)-radical SMMs, where the exchange bias can shift QTM from zero-field, allowing thermal relaxation pathways to dominate, which we believe could be utilized in tetrahalosemiquinonate compounds of other Ln(III) ions. Additionally, weak intermolecular exchange interactions are observed for both analogues at $T < 10$ K.

Despite Gd(III) being magnetically isotropic to the first order, compound **1** exhibits an out-of-phase component in the ac magnetic susceptibility at low temperatures indicative of slow magnetic relaxation, which is consistent with a small number of other reported Gd(III) compounds.[47–49] Compound **2**, however, exhibits no slow magnetic relaxation in the measured field range. The difference in behavior between the two

analogues is likely due to the different intermolecular interactions arising from the different crystal packing of the two compounds. The observation of slow magnetic relaxation is relatively unusual for Gd(III) complexes due to their near negligible anisotropy, although it has been observed for several other Gd species to date. Additionally, recent studies have shown long coherence times for several Gd-SMMs in pulsed EPR experiments, opening up applications for their use as qubits in quantum computing and highlighting the need for further investigations into the origins of slow magnetic relaxation in Gd(III) compounds.[49,51]

Experimental Section

Synthetic procedures: Tetrabromo-1,2-catechol was synthesized as previously reported.[65] The catecholate precursors [Ln(18-c-6)X_4Cat-(NO_3)].MeCN (**1-Cat**: X = Cl; **2-Cat**: X = Br) were prepared according to the literature procedures.[30] Tetrabutylammonium triiodide was synthesized according to the literature procedure.[66] All other chemicals were purchased from commercial suppliers and used without further purification.

Synthesis of [Gd(18-c-6)Cl_4SQ(NO_3)].I_3 (1): Solid **1-Cat** (190 mg, 0.25 mmol) was immersed in a 0.01 M I_2 solution in chlorobenzene (38 mL, 1.5 equiv.) for 4 hours, at which point the solid compound had changed color to a dark brown solid. The solid was collected by vacuum filtration, washed with cold chlorobenzene and diethyl ether, and air dried. The crude solid was then dissolved in dry, degassed dichloromethane (15 mL). Any undissolved solid was removed by filtration, and dry, degassed chlorobenzene (10 mL) added. The solution volume was reduced by 50%, and the solution was stored under nitrogen at −18 °C for up to a week, and the resulting dark brown microcrystalline solid collected by vacuum filtration, washed with cold chlorobenzene and diethyl ether and air dried, yielding compound **1** (145 mg, 53%). Selected FT-IR data for **1** (ATR): 2941 (w), 1541 (m), 1451 (s), 1292 (m), 1245 (m), 1212 (w), 1063 (s), 960 (s), 835 (w), 783 (m), 742 (w), 682 (w), 581 (w), 470 (m) cm^{-1}; UV/Vis/NIR (acetonitrile): λ_{max} (ε) = 229 (27,800), 288 (44,000), 360 (18,300), 934 nm (258 $mol^{-1}Lcm^{-1}$); elemental analysis calcd (%) for $C_{18}H_{23}Cl_4GdI_3NO_{11}$: C 19.47 H 2.18, N 1.26; found: C 19.83, H 2.11, N 1.12.

Synthesis of [Gd(18-c-6)Br_4SQ(NO_3)].I_3 (2): Solid **2-Cat** (335 mg, 0.36 mmol) was immersed in a 0.01 M I_2 solution in chlorobenzene (70 mL, 1.5 equiv.) for 4 hours, at which point the solid compound had changed color to a black solid. The solid was collected by vacuum filtration, washed with cold chlorobenzene and diethyl ether, and air dried. The crude solid was then dissolved in dichloromethane (30 mL). Any undissolved solid was removed by filtration and chlorobenzene (10 mL) added. The solution volume was reduced by 50% and was left at −18 °C for up to a week to crystallize. The resulting black crystalline solid was collected by vacuum filtration, washed with cold chlorobenzene and diethyl ether and air dried, yielding **2** (193 mg, 42%). Selected FT-IR data for **2** (ATR): 2938 (w), 1537 (m), 1508 (s), 1455 (s), 1278 (m), 1249 (w), 1067 (s), 960 (s), 835 (m), 734 (m), 608 (w), 470 (w) cm^{-1}; UV/Vis/NIR (acetonitrile): λ_{max} (ε) = 212 (28,000), 223 (27,400), 291 (40,100), 360 (19,700), 920 nm (196 $mol^{-1}Lcm^{-1}$); elemental analysis calcd (%) for $C_{18}H_{23}Br_4GdI_3NO_{11}$: C 16.79 H 1.88, N 1.09; found: C 17.12, H 1.77, N 1.58.

X-ray diffraction and structure solution: All X-ray diffraction data were obtained on an XtaLAB Synergy-S diffractometer from Rigaku Oxford Diffraction with a HyPix-6000HE detector, with data for compound **1** collected with Cu–Kα (λ = 1.5406 Å) radiation and data for compound **2** with Mo–Kα (λ = 0.71073 Å) radiation. All X-ray diffraction data were collected at 100 K. Deposition Numbers CCDC 2163212 and 2163213 contain the supplementary crystallographic data for this paper. These data are provided free of charge by the joint Cambridge Crystallographic Data Centre and Fachinformationszentrum Karlsruhe Access Structures service.

Single crystal X-ray diffraction data were reduced using CrysalisPro[67] and corrected using a numerical absorption correction based on Gaussian integration over a multi-faceted crystal model. Crystals used for single crystal X-ray diffraction were transferred directly from solution to crystallographic oil to prevent solvent loss. All structures were solved with the SHELXT[68] structure solution program using Intrinsic Phasing and refined with the SHELXL[69] refinement package using least squares minimization on all data, in Olex2.[70] All non-hydrogen atoms were refined with anisotropic displacement parameters, and all hydrogen atoms were placed at geometrical estimates and refined using the riding model.

Samples for powder X-ray diffraction were lightly crushed and loaded into 3 mm borosilicate glass capillaries for measurement. A Gandolfi move for powders was used with data collected to 2θ = 70°. Powder X-ray diffraction data were simulated from the single crystal X-ray structures using the software Mercury.[71]

Magnetic measurements: Magnetic measurements on microcrystalline powder samples were measured on a Quantum Design PPMS magnetometer with an ac Measurement System (ACMS) insert. Samples were measured in gelatin capsules, restrained in eicosane wax to prevent magnetic torquing. Ferromagnetic checks were performed on all samples to check for ferromagnetic impurities. Static susceptibility and magnetization data were corrected for the diamagnetic contribution of the gelatin capsule and eicosane, as well as the diamagnetic contribution of the samples, using Pascals constants.[72] Magnetic measurements on frozen solutions were measured on a Quantum Design MPMS 3 SQUID magnetometer. Samples were prepared as 20 mM 1:1 MeCN:toluene solutions in flame sealed borosilicate NMR tubes and flash frozen.

Electron paramagnetic resonance: Electron paramagnetic resonance measurements were performed on microcrystalline powders of **1** and **2** at 5 K with X-band microwave radiation (ν = 9.41 GHz) using a Bruker E500 spectrometer equipped with an ESR900 (Oxford Instruments) continuous flow ^{4}He cryostat and a SHQ resonator. The EPR data was simulated in PHI[44] using an isotropic linewidth of 3 GHz.

Physical properties & characterization: Cyclic voltammetry (CV) and rotating disk electrode (RDE) voltammetry were performed on 10^{-3} M solutions under an N_2 atmosphere. For CV a 1 mm diameter glassy carbon was used as the working electrode, while for RDE voltammetry a 3 mm glassy carbon electrode was used. For all measurements, a Pt coated Ti wire was used as the counter electrode and a leakless Ag/AgCl electrode as the reference electrode. The ferrocene/ferrocenium (Fc/Fc^+) couple was used as an internal reference.

UV-visible spectra were measured on an Agilent Technology Cary 60 UV-Visible spectrometer and Vis-NIR spectra were measured on a PerkinElmer UV-Vis-NIR Spectrometer Lambda 1050. Fourier transform infrared (FT-IR) spectra were obtained as attenuated total reflectance (ATR) on a Bruker Alpha FT-IR spectrometer and normalized as absorbance spectra. Elemental (CHN) analyses were performed at the Campbell Microanalytical Laboratory, University of Otago.

Acknowledgements

M. A. D. acknowledges financial support from AINSE Limited (AINSE Post-Graduate Research Award) and the Australian Government for a Research Training Program stipend. C.B., and R.A.M. thank the Australian Research Council for funding (DP170100034 and LE210100009). We acknowledge the support of the Australian Centre for Neutron Scattering, Australian Nuclear Science and Technology Organisation and the Australian Government through the National Collaborative Research Infrastructure Strategy. L. S. acknowledges the financial support of the Italian Ministry of Education, University and Research (MIUR), for the economic contribution within the "Progetto Dipartimenti di Eccellenza 2018-2022" allocated to the Department of Chemistry "Ugo Schiff" (ref B96C1700020008). The authors would like to thank Dr Moya A. Hay and Dr Marcus J. Giansiracusa for helpful discussions. Open access publishing facilitated by The University of Melbourne, as part of the Wiley - The University of Melbourne agreement via the Council of Australian University Librarians.

Conflict of Interest

The authors declare no conflict of interest.

Data Availability Statement

The data that support the findings of this study are available from the corresponding author upon reasonable request.

Keywords: exchange interactions · electron paramagnetic resonance · lanthanides · magnetic properties · relaxation

[1] A. V. Pavlishchuk, V. V. Pavlishchuk, *Theor. Exp. Chem.* **2020**, *56*, 1–25.
[2] M. Bottrill, L. Kwok, N. J. Long, *Chem. Soc. Rev.* **2006**, *35*, 557.
[3] D. Parker, E. A. Suturina, I. Kuprov, N. F. Chilton, *Acc. Chem. Res.* **2020**, *53*, 1520–1534.
[4] M. J. Giansiracusa, G. K. Gransbury, N. F. Chilton, D. P. Mills, in *Encycl. Inorg. Bioinorg. Chem.* (Ed.: R. A. Scott), John Wiley & Sons Ltd, Chichester West Sussex, UK, **2021**, p. eibc2784.
[5] D. N. Woodruff, R. E. P. Winpenny, R. A. Layfield, *Chem. Rev.* **2013**, *113*, 5110–5148.
[6] P. Zhang, L. Zhang, J. Tang, *Dalton Trans.* **2015**, *44*, 3923–3929.
[7] F. Guo, B. M. Day, Y. Chen, M.-L. Tong, A. Mansikkamäki, R. A. Layfield, *Science* **2018**, *362*, 1400–1403.
[8] C. A. Gould, K. R. McClain, D. Reta, J. G. C. Kragskow, D. A. Marchiori, E. Lachman, E. Choi, J. G. Analytis, R. D. Britt, N. F. Chilton, B. G. Harvey, J. R. Long, *Science* **2022**, *375*, 198–202.
[9] D. Gatteschi, R. Sessoli, L. Sorace, in *Handb. Phys. Chem. Rare Earths, Vol. 50* (Eds.: J.-C. G. Bünzli, V. K. Pecharsky), Elsevier, Amsterdam, **2016**, pp. 91–139.
[10] S. Demir, I.-R. Jeon, J. R. Long, T. D. Harris, *Coord. Chem. Rev.* **2015**, *289–290*, 149–176.
[11] S. Demir, M. I. Gonzalez, L. E. Darago, W. J. Evans, J. R. Long, *Nat. Commun.* **2017**, *8*, 2144.
[12] L. Zhang, Y.-Q. Zhang, P. Zhang, L. Zhao, M. Guo, J. Tang, *Inorg. Chem.* **2017**, *56*, 7882–7889.
[13] T. Morita, M. Damjanović, K. Katoh, Y. Kitagawa, N. Yasuda, Y. Lan, W. Wernsdorfer, B. K. Breedlove, M. Enders, M. Yamashita, *J. Am. Chem. Soc.* **2018**, *140*, 2995–3007.
[14] C. Benelli, A. Caneschi, D. Gatteschi, J. Laugier, P. Rey, *Angew. Chem. Int. Ed.* **1987**, *26*, 913–915; *Angew. Chem.* **1987**, *99*, 958–959.
[15] J.-P. Sutter, M. L. Kahn, S. Golhen, L. Ouahab, O. Kahn, *Chem. Eur. J.* **1998**, *4*, 571–576.
[16] J.-X. Xu, Y. Ma, G.-F. Xu, C. Wang, D.-Z. Liao, Z.-H. Jiang, S.-P. Yan, L.-C. Li, *Inorg. Chem. Commun.* **2008**, *11*, 1356–1358.
[17] N. Ikegaya, T. Kanetomo, R. Murakami, T. Ishida, *Chem. Lett.* **2012**, *41*, 82–83.
[18] C. Lescop, D. Luneau, E. Belorizky, P. Fries, M. Guillot, P. Rey, *Inorg. Chem.* **1999**, *38*, 5472–5473.
[19] J. D. Rinehart, M. Fang, W. J. Evans, J. R. Long, *Nat. Chem.* **2011**, *3*, 538–542.
[20] Y.-L. Wang, Y.-Y. Gao, Y. Ma, Q.-L. Wang, L.-C. Li, D.-Z. Liao, *J. Solid State Chem.* **2013**, *202*, 276–281.
[21] S. Demir, M. Nippe, M. I. Gonzalez, J. R. Long, *Chem. Sci.* **2014**, *5*, 4701–4711.
[22] T. Kanetomo, T. Ishida, *Inorg. Chem.* **2014**, *53*, 10794–10796.
[23] C. A. Gould, J. Marbey, V. Vieru, D. A. Marchiori, R. David Britt, L. F. Chibotaru, S. Hill, J. R. Long, *Nat. Chem.* **2021**, *13*, 1001–1005.
[24] T. Tezgerevska, K. G. Alley, C. Boskovic, *Coord. Chem. Rev.* **2014**, *268*, 23–40.
[25] M. G. Chegerev, A. A. Starikova, *Eur. J. Inorg. Chem.* **2021**, *2021*, 2684–2695.
[26] M. A. Dunstan, E. Rousset, M.-E. Boulon, R. W. Gable, L. Sorace, C. Boskovic, *Dalton Trans.* **2017**, *46*, 13756–13767.
[27] W. R. Reed, M. A. Dunstan, R. W. Gable, W. Phonsri, K. S. Murray, R. A. Mole, C. Boskovic, *Dalton Trans.* **2019**, *48*, 15635–15645.
[28] P. Zhang, M. Perfetti, M. Kern, P. P. Hallmen, L. Ungur, S. Lenz, M. R. Ringenberg, W. Frey, H. Stoll, G. Rauhut, J. van Slageren, *Chem. Sci.* **2018**, *9*, 1221–1230.
[29] M. Dunstan, M. Cagnes, W. Phonsri, K. Murray, R. A. Mole, C. Boskovic, *Aust. J. Chem.* **2022**, doi: 10.1071/CH21306.
[30] E. Rousset, M. Piccardo, M.-E. Boulon, R. W. Gable, A. Soncini, L. Sorace, C. Boskovic, *Chem. Eur. J.* **2018**, *24*, 14768–14785.
[31] D. I. Alexandropoulos, L. Cunha-Silva, G. Lorusso, M. Evangelisti, J. Tang, T. C. Stamatatos, *Chem. Commun.* **2016**, *52*, 1693–1696.
[32] G. V. Romanenko, S. V. Fokin, G. A. Letyagin, A. S. Bogomyakov, V. I. Ovcharenko, *J. Struct. Chem.* **2019**, *60*, 1091–1100.
[33] E. Rousset, R. W. Gable, A. Starikova, C. Boskovic, *Cryst. Growth Des.* **2020**, *20*, 3396–3405.
[34] N. A. Pushkarevsky, M. A. Ogienko, A. I. Smolentsev, I. N. Novozhilov, A. Witt, M. M. Khusniyarov, V. K. Cherkasov, S. N. Konchenko, *Dalton Trans.* **2016**, *45*, 1269–1278.
[35] D. M. Kuzyaev, D. L. Vorozhtsov, N. O. Druzhkov, M. A. Lopatin, E. V. Baranov, A. V. Cherkasov, G. K. Fukin, G. A. Abakumov, M. N. Bochkarev, *J. Organomet. Chem.* **2012**, *698*, 35–41.
[36] A. Caneschi, A. Dei, D. Gatteschi, L. Sorace, K. Vostrikova, *Angew. Chem. Int. Ed.* **2000**, *39*, 246–248; *Angew. Chem.* **2000**, *112*, 252–254.
[37] A. Caneschi, A. Dei, D. Gatteschi, S. Poussereau, L. Sorace, *Dalton Trans.* **2004**, *24*, 1048–1055.
[38] P. Llunell, M. Casanova, D. Cirera, J. Bofill, J. M. Alemany, D. Alvarez, S. Pinsky, M. Avnir, *SHAPE 2.1*, Universitat de Barcelona and The Hebrew University of Jerusalem, **2003**.
[39] S. N. Brown, *Inorg. Chem.* **2012**, *51*, 1251–1260.
[40] C. G. Pierpont, *Inorg. Chem.* **2011**, *50*, 9766–9772.
[41] P. B. Chatterjee, K. Bhattacharya, N. Kundu, K.-Y. Choi, R. Clérac, M. Chaudhury, R. Clérac, M. Chaudhury, *Inorg. Chem.* **2009**, *48*, 804–806.
[42] G. Ulas, T. Lemmin, Y. Wu, G. T. Gassner, W. F. DeGrado, *Nat. Chem.* **2016**, *8*, 354–359.
[43] A. Caneschi, A. Dei, D. Gatteschi, C. A. Massa, L. A. Pardi, S. Poussereau, L. Sorace, *Chem. Phys. Lett.* **2003**, *371*, 694–699.
[44] N. F. Chilton, R. P. Anderson, L. D. Turner, A. Soncini, K. S. Murray, *J. Comput. Chem.* **2013**, *34*, 1164–1175.
[45] R. M. Buchanan, S. L. Kessel, H. H. Downs, C. G. Pierpont, D. N. Hendrickson, *J. Am. Chem. Soc.* **1978**, *100*, 7894–7900.
[46] M. W. Lynch, R. M. Buchanan, C. G. Pierpont, D. N. Hendrickson, *Inorg. Chem.* **1981**, *20*, 1038–1046.
[47] Y. Horii, K. Katoh, Y. Miyazaki, M. Damjanović, T. Sato, L. Ungur, L. F. Chibotaru, B. K. Breedlove, M. Nakano, W. Wernsdorfer, M. Yamashita, *Chem. Eur. J.* **2020**, *26*, 8076–8082.
[48] M. Orendáč, L. Sedláková, E. Čižmár, A. Orendáčová, A. Feher, S. A. Zvyagin, J. Wosnitza, W. H. Zhu, Z. M. Wang, S. Gao, *Phys. Rev. B* **2010**, *81*, 214410.
[49] M. J. Martínez-Pérez, S. Cardona-Serra, C. Schlegel, F. Moro, P. J. Alonso, H. Prima-García, J. M. Clemente-Juan, M. Evangelisti, A. Gaita-Ariño, J.

Sesé, J. van Slageren, E. Coronado, F. Luis, *Phys. Rev. Lett.* **2012**, *108*, 247213.
[50] T. T. da Cunha, V. M. M. Barbosa, W. X. C. Oliveira, C. B. Pinheiro, E. F. Pedroso, W. C. Nunes, C. L. M. Pereira, *Polyhedron* **2019**, *169*, 102–113.
[51] G. Handzlik, M. Magott, M. Arczyński, A. M. Sheveleva, F. Tuna, M. Sarewicz, A. Osyczka, M. Rams, V. Vieru, L. F. Chibotaru, D. Pinkowicz, *J. Phys. Chem. Lett.* **2020**, *11*, 1508–1515.
[52] T. K. Ghosh, S. Maity, J. Mayans, A. Ghosh, *Inorg. Chem.* **2021**, *60*, 438–448.
[53] A. Vráblová, M. Tomás, L. R. Falvello, Ľ. Dlháň, J. Titiš, J. Černák, R. Boča, *Dalton Trans.* **2019**, *48*, 13943–13952.
[54] G. Handzlik, M. Magott, M. Arczyński, A. M. Sheveleva, F. Tuna, S. Baran, D. Pinkowicz, *Dalton Trans.* **2020**, *49*, 11942–11949.
[55] T. Yoshida, G. Cosquer, D. C. Izuogu, H. Ohtsu, M. Kawano, Y. Lan, W. Wernsdorfer, H. Nojiri, B. K. Breedlove, M. Yamashita, *Chem. Eur. J.* **2017**, *23*, 4551–4556.
[56] R. J. Holmberg, L. T. A. Ho, L. Ungur, I. Korobkov, L. F. Chibotaru, M. Murugesu, *Dalton Trans.* **2015**, *44*, 20321–20325.
[57] D. C. Izuogu, T. Yoshida, H. Zhang, G. Cosquer, K. Katoh, S. Ogata, M. Hasegawa, H. Nojiri, M. Damjanović, W. Wernsdorfer, T. Uruga, T. Ina, B. K. Breedlove, M. Yamashita, *Chem. Eur. J.* **2018**, *24*, 9285–9294.
[58] C. E. Jackson, I. P. Moseley, R. Martinez, S. Sung, J. M. Zadrozny, *Chem. Soc. Rev.* **2021**, *50*, 6684–6699.
[59] M. Vonci, M. J. Giansiracusa, R. W. Gable, W. Van den Heuvel, K. Latham, B. Moubaraki, K. S. Murray, D. Yu, R. A. Mole, A. Soncini, C. Boskovic, *Chem. Commun.* **2016**, *52*, 2091–2094.
[60] S. Liu, J. Lu, X.-L. Li, Z. Zhu, J. Tang, *Dalton Trans.* **2020**, *49*, 12372–12379.
[61] J. Flores Gonzalez, V. Montigaud, V. Dorcet, K. Bernot, B. Le Guennic, F. Pointillart, O. Cador, *Chem. Eur. J.* **2021**, *27*, 10160–10168.
[62] K. S. Pedersen, L. Ungur, M. Sigrist, A. Sundt, M. Schau-Magnussen, V. Vieru, H. Mutka, S. Rols, H. Weihe, O. Waldmann, L. F. Chibotaru, J. Bendix, J. Dreiser, *Chem. Sci.* **2014**, *5*, 1650–1660.
[63] P. Cen, Z. He, R. Ding, H. Yang, L. Li, Y.-Q. Zhang, Y. Li, D. Tian, X. Liu, *CrystEngComm* **2021**, *23*, 5443–5450.
[64] A. Dei, D. Gatteschi, J. Pécaut, S. Poussereau, L. Sorace, K. Vostrikova, *C. R. Acad. Sci., Ser. II.* **2001**, *4*, 135–141.
[65] A. Menzek, H. T. Balaydın, Y. Akbaba, E. Şahin, S. Göksu, *Arkivoc* **2010**, *2009*, 75–87.
[66] R. E. Buckles, J. P. Yuk, *J. Am. Chem. Soc.* **1953**, *75*, 5048–5052.
[67] Agilent (**2014**). CrysAlis PRO. Agilent Technologies Ltd, Yarnton, Oxfordshire, England.
[68] G. M. Sheldrick, *Acta Crystallogr. Sect. A* **2015**, *71*, 3–8.
[69] G. M. Sheldrick, *Acta Crystallogr. Sect. C* **2015**, *71*, 3–8.
[70] O. V. Dolomanov, L. J. Bourhis, R. J. Gildea, J. A. K. Howard, H. Puschmann, *J. Appl. Crystallogr.* **2009**, *42*, 339–341.
[71] C. F. Macrae, I. Sovago, S. J. Cottrell, P. T. A. Galek, P. McCabe, E. Pidcock, M. Platings, G. P. Shields, J. S. Stevens, M. Towler, P. A. Wood, *J. Appl. Crystallogr.* **2020**, *53*, 226–235.
[72] G. A. Bain, J. F. Berry, *J. Chem. Educ.* **2008**, *85*, 532.

Manuscript received: March 31, 2022
Revised manuscript received: May 26, 2022
Accepted manuscript online: May 29, 2022
Version of record online: June 20, 2022